Copper precipitation in FeCu, FeCuMn, and FeCuNi dilute alloys followed by X-ray absorption spectroscopy

1994 J. Phys.: Condens. Matter 6 569

(http://iopscience.iop.org/0953-8984/6/2/027)

J. Phys.: Condens. Matter 6 (1994) 569–588. Printed in the UK

Copper precipitation in FeCu, FeCuMn, and FeCuNi dilute alloys followed by x-ray absorption spectroscopy

F Maury†, N Lorenzelli†, M H Mathon†, C H de Novion† and P Lagarde‡

† Laboratoire des Solides Irradiés, Ecole Polytechnique, F-91128 Palaiseau Cédex, France
‡ LURE, Bâtiment 209, Université Paris-Sud, F-91405 Orsay, France

Received 4 August 1993, in final form 24 September 1993

Abstract. Samples of FeCu, FeCuMn, FeCuNi, and FeCuCr alloys containing 1.5 wt% of each solute have been electron irradiated around 290 °C or thermally aged at 500 °C for various times. It is known that such treatments induce Cu precipitation; the Cu depletion of the matrix is measured by the resistivity decrease of the samples. The crystallographic environment of the solute atoms in the irradiated or aged samples has been studied by XAS (x-ray absorption spectroscopy).

The data show that Cr, Mn, and Ni atoms mainly remain in BCC solid solution during the Cu precipitation. The first Cu precipitates are found to be of BCC structure, i.e. coherent with the matrix. At the longest ageing times, they have become of FCC structure. In the electron-irradiated samples, the data show that, up to a fluence of 5 C cm^{-2}, most of the Cu precipitates (> 80%) are still of BCC structure.

The fraction of BCC precipitates has been estimated from both the x-ray-absorption near-edge structure (XANES) and extended x-ray-absorption fine-structure (EXAFS) data. It appears that, for both FeCu and FeCuMn samples, similarly aged, the FCC fraction is larger in cold-rolled samples than in pre-annealed and quenched ones.

The results obtained are consistent, in the FeCu case, with a simple linear correspondence between fluence and time, 1 C cm^{-2} at 300 °C being equivalent to ~ 10 h at 500 °C. The Cu precipitation is found to be accelerated, at least in its first stages, by the presence of Mn in the alloy.

1. Introduction

The present work takes place in an extensive study of the embrittlement processes occurring in nuclear-reactor pressure-vessel steels under their usual operating conditions (Soulat and Meyzaud 1990). This embrittlement is known to depend strongly on the residual impurity content of the steel, the Cu playing a major role (Little 1983). It has been shown (Frisius and Bünemann 1979, Beaven *et al* 1986) that the Cu atoms, initially in metastable solid solution in the BCC Fe matrix (the solubility of Cu in Fe is less than 0.1% below 550 °C), precipitate under neutron irradiation at temperatures around 300 °C as during thermal ageing at temperatures $\geqslant$ 500 °C. This precipitation hardens the material and therefore contributes to its embrittlement. Hardness is found to increase, both for thermally aged samples and irradiated ones (Phythian *et al* 1990); for thermally aged samples, it goes through a maximum as ageing proceeds (Hornbogen and Glenn 1960, Worrall *et al* 1987). Other solutes such as Ni, Mn, and Cr have been suspected to play a role in the Cu precipitation, either by co-precipitating with the Cu atoms or by hindering the Cu precipitation. The XAS technique enables us to follow the solute precipitation since it provides some information on the nearest neighbours of the solute atoms.

0953-8984/94/020569+20$07.50

The present study was limited to model alloys containing 1.5% of solute, a concentration higher than that effectively encountered in the vessel steels (typically 0.1%, eventually up to 0.6%). More dilute alloys together with real steels aged in operating reactors have been studied by other techniques, such as resistivity, micro-hardness, small-angle neutron-scattering (SANS) measurements (Barbu *et al* 1992); a solute concentration of about 1.5% is, however, a lower limit for an absorption x-ray study where the contribution of the matrix to the signal is not zero.

These model alloys were electron irradiated at different temperatures, mostly around 290 °C, which is the working temperature of the pressurized-water nuclear reactors. The electronic irradiation has been chosen to yield simple Frenkel defects and to facilitate a first approach of modellization. Moreover it leads to much more rapid structural changes than those taking place in the reactors, thus making the experiment possible. The same alloys were also thermally aged at 500 °C for various times in order to provide a comparison between irradiation and thermal ageing.

A first EXAFS (extended x-ray-absorption fine-structure) study by Pizzini *et al* (1990) has shown that in the model alloys Fe–1.3% Cu and Fe–1.3% Cu–1.4% Ni thermally aged at 550 °C, the Cu precipitates in the peak hardness condition (2 h at 550 °C) have a BCC structure. From a preliminary XANES (x-ray absorption near-edge structure) and EXAFS study, we reached the same conclusion for thermally aged Fe–1.3% Cu–0.5% Mn (Maury *et al* 1991b). The precipitate transformation from the BCC structure to the FCC one has been shown recently by transmission electron microscopy (Othen *et al* 1991) to occur, in thermally aged FeCu and FeCuNi, through an intermediate 9R phase (the 9R phase is similar to the FCC phase, except that the stacking sequence of close-packed planes is ABC BCA CAB ... instead of ABC ABC ...). Up to now no XAS data have been available for irradiated samples.

We present, in sections 3 and 4 respectively, the XANES and EXAFS results at the different thresholds (Cu, Mn,...). The data are analysed quantitatively in section 5; the analysis yields an estimate of the fraction of BCC precipitates. Finally the results are compared to other experimental data and discussed in section 6.

2. Experimental details

2.1. Samples

The FeCu and FeCuMn alloys were elaborated by the LETRAM/SRMA, CE, Saclay. A chemical analysis yielded the following composition: 1.34 ± 0.04 at.% Cu for FeCu; 1.26 ± 0.02 at.% Cu and 1.37 ± 0.03 at.% Mn for FeCuMn. The residual impurity content of the basis material was 0.20 ± 0.01 at.% Al, 0.045 ± 0.01 at.% C and 0.04 ± 0.04 at.% Si.

The FeCuNi (1.5 at.% Cu, 1.5 at.% Ni) and FeCuCr (1.5 at.% Cu, 2.25 at.% Cr) alloys were fabricated by the CECM, CNRS, Vitry. No analysis is available for these alloys, but the levitation procedure used provides much purer materials. A typical analysis of such materials yields a concentration of Si (main residual impurity) $\simeq$ 20 at. ppm and a C concentration $\leqslant$ 5 at. ppm.

The starting material was cold rolled down to a thickness of $\sim$ 25 μm, cut to size ($\sim 1.2 \times 3$ cm^2 for the irradiated samples and 1.5×1.5 cm^2 for the thermally aged samples) and cleansed in an $H_2O_2 + 5\%$ HF bath. Most of the samples were aged after having been pre-annealed for 24 h under H_2 at 820 °C (800 °C for a couple of FeCuMn samples) and quenched from the annealing temperature. The grain size was $\sim$ 50 μm. These samples

will be labelled AQ in the following. Some samples were aged directly from the cold-rolled state; they will be labelled CR.

Thermal ageing was performed under H_2 at a temperature of 500 °C and for various ageing times between 2.5 and 312 h.

Finally the C content of the **FeCu** and **FeCuMn** samples was determined by a combustion and conductimetry analysis. It was found to be smaller than the lower detectable limit (90 at. ppm) in all **FeCu** samples except for the cold-rolled ones. In this sample, it was, as expected, 600 at. ppm. The precision of the analysis was somewhat better for the **FeCuMn** samples. The C content of the cold-rolled **FeCuMn** sample was surprisingly found to be less than 50 at. ppm. That of all other samples (quenched, thermally aged, irradiated), was found to lie between less than 50 and about 150 at. ppm, being not quite constant inside a given sample.

2.2. Irradiation

The irradiation runs were performed with the Van de Graaff accelerator of Ecole Polytechnique, Palaiseau. The electron energy was 2.5 MeV. The sample chamber was filled with He at a pressure of 1.15 bar and the irradiation temperature maintained around 290 °C by controlling the incident electron flux. The XAS samples were mounted into a sandwich of two thicker samples of the same nature, which allowed the sample temperature to attain its fixed value for reachable values of the electron flux ($\sim 5 \times 10^{13}$ e^- cm^{-2} s^{-1}).

Three thin thermocouples (copper/constantan) were soldered onto the irradiated samples, one in the middle of the irradiated area ($\sim$ 15 mm long), the two others at each end of the sample (3 cm long), outside the irradiated area. The temperature difference between the centre and the extremities of the sample was $\sim$ 50 °C; we ensured by a simple estimation that the temperature was homogeneous throughout the irradiated area within a few degrees.

The temperature of the central part of the sample ($\sim$ 7 mm long) was checked by recording its electrical resistivity under irradiation (Lé 1992). The two measurements (resistivity and thermocouple) were found to coincide within about 5 °C.

The solute depletion of the matrix was followed by measuring the sample resistivity as a function of the electron fluence at a reference temperature of 30 °C (Lé 1992). As concerns the resistivity, not much difference was found between the **FeCu** and **FeCuMn** samples, either cold rolled or pre-annealed and quenched. A bigger difference (see figure 1) was found between cold-rolled samples on one hand and annealed/quenched samples on the other, either **FeCu** or **FeCuMn**. This is an indication that the dislocation content of the sample may play a more important role than its residual C content.

The resistivity of the **FeCu** and **FeCuMn** alloys was found to decrease less rapidly with the electron fluence than that of the purer **FeCuNi** and **FeCuCr** alloys, which can be attributed to the influence of the residual impurities.

2.3. X-ray absorption measurements

The x-ray absorption coefficient μ of the samples was measured near and above the Cu K edge (and also near and above the Mn K edge for **FeCuMn** samples, the Ni K edge for **FeCuNi** samples and the Cr K edge for **FeCuCr** samples).

The measurements were performed at room temperature at the EXAFS I and III stations of LURE, Orsay, using the x-ray beam delivered by the DCI storage ring running typically at 1.85 GeV and 300 mA. The Bragg monochromator was an Si channel-cut device with a (331) cut for EXAFS I and a two-crystal Si (311) device for EXAFS III. The incident and transmitted x-ray fluxes, I_0 and I respectively, were measured by two ionization chambers

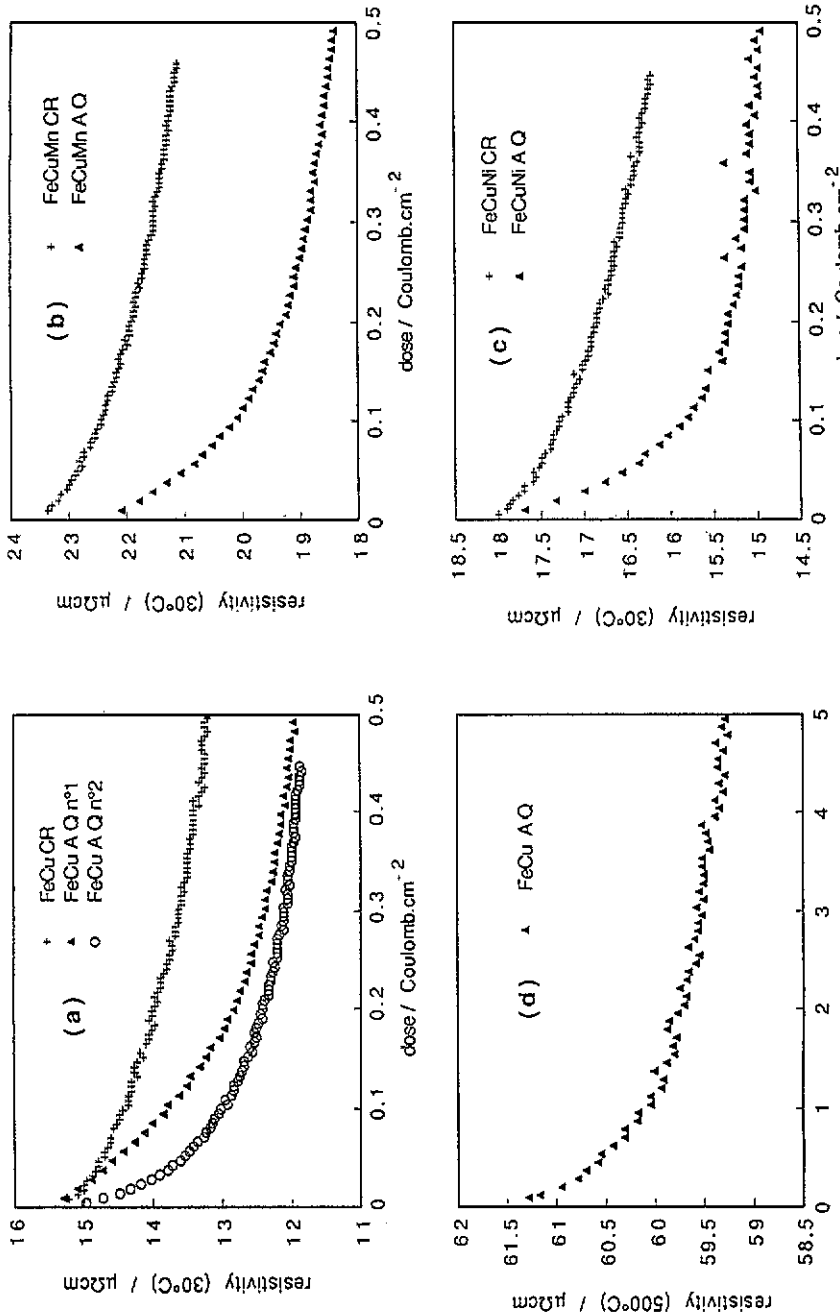

Figure 1. Sample electrical resistivity measured at 30 °C as a function of the fluence for the three alloys FeCu (*a*), FeCuMn (*b*), and FeCuNi (*c*), and measured at 500 °C as a function of the ageing time for FeCu (*d*). CR stands for cold rolled, AQ for pre-annealed and quenched. FeCu AQ No 1 has been pre-annealed at 820 °C under static H_2. FeCu AQ No 2 pre-annealed at 830 °C under flowing H_2.

filled with air. The photon energy was swept throughout a 600 keV range by steps of 4 eV below the threshold, 0.3 eV in the threshold region (the XANES range) and 1 eV above the threshold (the EXAFS range).

3. XANES results

It has been shown (Müller *et al* 1978, 1982) that in the case of 4d and 3d transition metals, the absorption coefficient μ in the range of a few tens of eV above the K absorption threshold is well explained, in a one-electron approximation, by the p partial density of states which itself depends on the crystallographic structure of the metal. More generally, this near-edge part of the x-ray spectrum is well known to depend strongly on the symmetry of the environment of the absorbing atom.

We thus should be able to gain some information, at least qualitative, on the structure of the crystal surrounding the atom that absorbs the incident photon (central atom), from the shape of the $\mu(E)$ curve just above the edge (Cu K edge for a Cu atom). However the shape of the curve can be perturbed by the presence of an oxide layer on the sample as has been observed in a previous experiment (Maury *et al* 1991b). For this reason, most of our irradiated samples were cleansed again after the irradiation run, although the thickness of the sample is then not so accurately defined.

3.1. Cu threshold

Figure 2 shows the absorption coefficient, $\mu(E) = \log(I_0/I)$, as a function of the photon energy near the Cu K edge, for thermally aged **Fe**Cu and **Fe**CuMn samples. A constant background, extrapolated from below the edge, has been subtracted from the measured μ values and the curves have been normalized to the height of the absorption step at the edge. For the sake of clarity not all the data are shown on the figure. Figure 3 shows the measured absorption for various irradiated **Fe**CuMn samples.

One can see from figure 2 that the shape of the $\mu(E)$ curves between 8980 and 9010 eV transforms progressively, as 500 °C thermal ageing goes on, from the shape of the curve for pure Fe (at the Fe K edge) to that for pure Cu: the starting material, either cold-rolled (CR) or pre-annealed and quenched (AQ), exhibits, like pure Fe, a unique bump around 8994 eV; this structure vanishes progressively as ageing proceeds and gives rise to two bumps around 8890 and 9000 eV, like those observed in pure Cu. As concerns the irradiated samples (see figure 3 for the **Fe**CuMn samples), the only apparent modification is the change in the shape of the first step around the Cu edge (8980 eV).

By comparing the experimental curves with calculated ones for given fractions of Cu atoms in BCC and FCC environments, one can estimate these fractions in the thermally aged or irradiated samples. The results are given in table 1 (AG stands for thermally aged at 500 °C). In this simple estimate, the existence of the 9R phase is not considered, i.e. it is assimilated to the FCC phase.

The data (see table 1 and figure 2) show that the BCC → FCC transformation is, for a given ageing time, more pronounced in CR than in AQ samples and more pronounced in **Fe**CuMn than in **Fe**Cu.

3.2. Cr, Mn, and Ni thresholds

The accuracy is better at the Cr and Mn threshold than at the Cu threshold since the Cr and Mn K edges lie below the Fe one. In contrast, it is worst at the Ni threshold, which

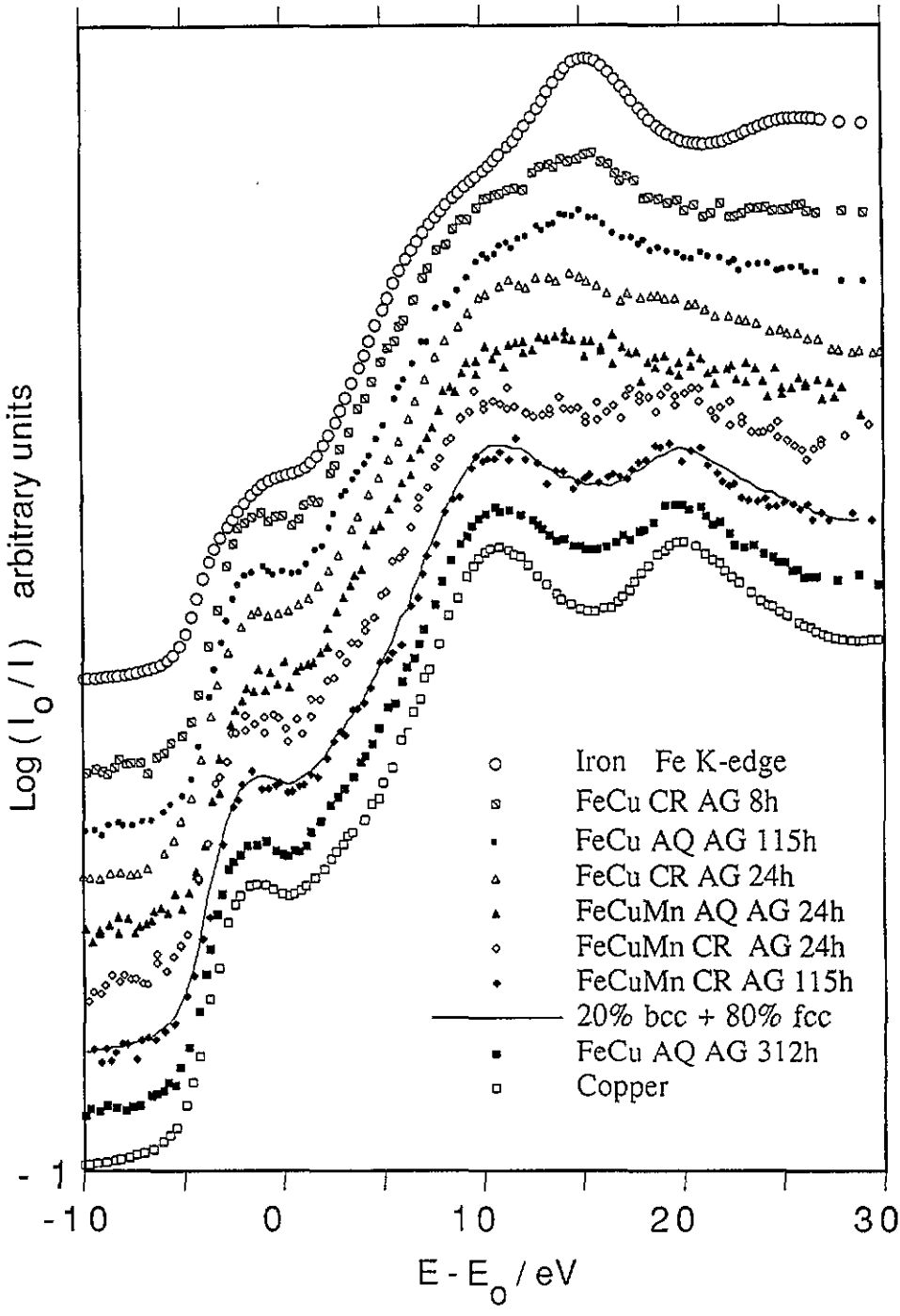

Figure 2. Absorption coefficient measured near the Cu K edge (or Fe K edge for Fe) for various thermally aged samples. CR stands for cold rolled, AQ for pre-annealed and quenched, AG for thermally aged at 500 °C. The symbols are measured data points; the curve is a mere linear combination of FeCuMn CR and Cu spectra.

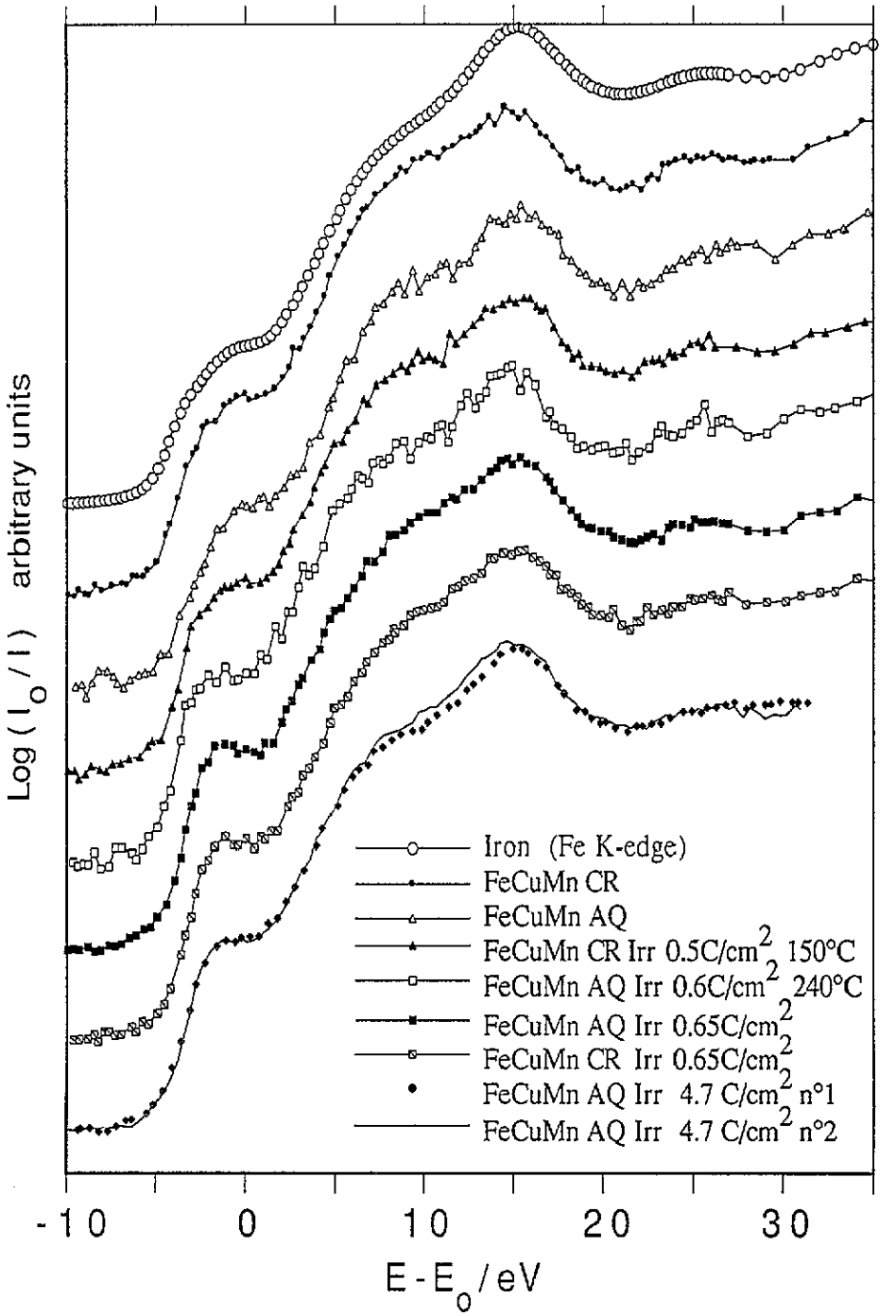

Figure 3. Absorption coefficient measured near the Cu K edge (or Fe K edge for Fe) for FeCuMn samples irradiated at 300 °C (except for the two cases where the irradiating temperature is displayed with the fluence). CR stands for cold rolled, AQ for pre-annealed and quenched.

Table 1. Fraction (in%) of Cu atoms in FCC environment estimated from the K Cu XANES data

Alloy	FeCu	FeCuNi	FeCuMn
Irradiated samples $T_{irr} \leq 300°C$; dose $<5C/cm^2$	0 - 20	0 - 20	0 - 20
A Q, AG 8h	10±10		
CR, AG 8h	25±10		
A Q, AG 24h		25±10	45±10[1]
CR, AG 24h	45±10		65±10
A Q, AG 67h, Irr[2]		50±10	
A Q, AG 115h	45±10		55±10[1]
A Q, AG 115h, Irr[3]			70±10
CR, AG 115h		70±10	80±5
A Q, AG 246h		70±10	
A Q, AG 312h	85±5		

[1] These samples have been pre-annealed at 800 °C.
[2] Sample e^- irradiated (0.65 C cm^{-2} at 270 °C) after thermal ageing.
[3] Sample e^- irradiated (0.55 C cm^{-2} at 240 °C) after thermal ageing.

lies just above the Fe one. For all studied samples, no change was detected even for the longest ageing times. Since all solute atoms contribute in the same way to the XAS signal, the present results only show that solutes other than Cu mainly remain in solid solution and do not enter significantly into the Cu precipitates.

4. EXAFS results

The EXAFS signal is defined as $\chi(E) = (\mu - \mu_0)/\mu_0$, with $I = I_0\, e^{-\mu x}$, x being the sample thickness; μ_0 is the atom-like smooth absorption above the edge. (Typical $\chi(E)$ curves for thermally aged FeCuMn alloys have been given previously (Maury *et al* 1991b)). This signal is divided by the edge step for normalization and Fourier transformed after multiplication by a Hanning function and by k^3 where k is the wave number of the photoelectron. Due to the low solute concentrations in our samples, we are near the accuracy limit of the method. Not all spectra could be exploited, depending on the sample thickness and thickness homogeneity. Moreover, even in the best cases, the amplitude of the EXAFS oscillations becomes rapidly small as compared to the dispersion of the data points; the workable energy range has to be limited: the Hanning function was chosen to be equal to zero outside an energy range of 25–530 (or 25–420) eV and equal to unity in an energy range of 40–430 (or 40–340) eV.

4.1. Cu threshold

Figures 4 and 5 show the Fourier transform (calculated with the smaller energy window) of the EXAFS spectra of, respectively, irradiated and thermally aged samples.

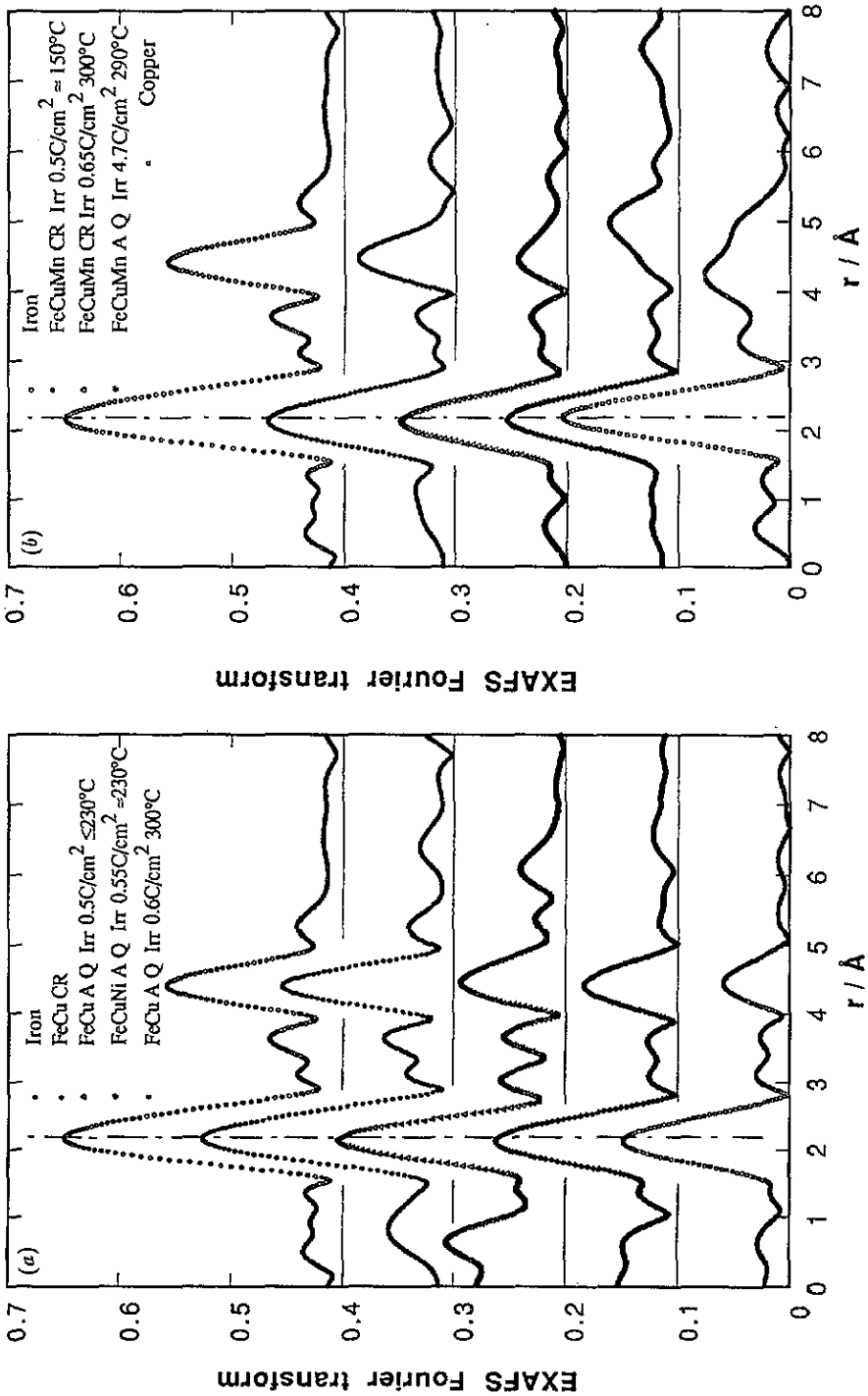

Figure 4. Fourier transform of the EXAFS spectrum for irradiated samples: (*a*) FeCu and FeCuNi, (*b*) FeCuMn. CR stands for cold rolled, AQ for pre-annealed and quenched. The irradiating temperature is given for each sample following the fluence.

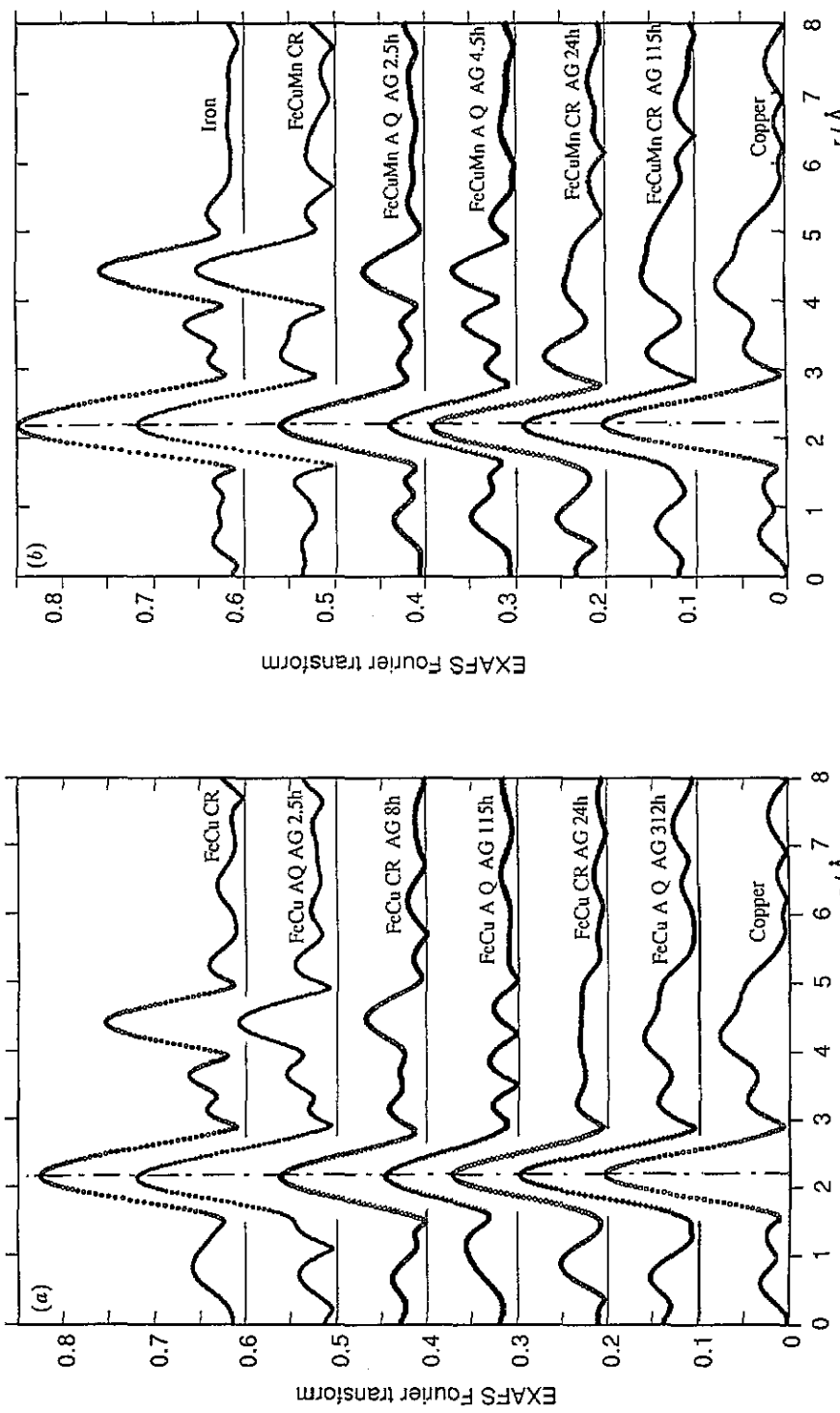

Figure 5. Fourier transform of the EXAFS *spectrum for thermally aged samples:(a)* **FeCu** *and (b)* **FeCuMn**. *The spectra of thermally aged* FeCuNi *samples are quite similar to those of* FeCu *and* FeCuMn *samples and not displayed on the figure.* CR *stands for cold rolled,* AQ *for pre-annealed and quenched.*

The spectra of the cold-rolled or quenched and annealed alloys show, as that of pure Fe (figures 4(*a*) and 5(*b*)), two large peaks centred around 2.2 and 4.4 Å. The first one, labelled peak I, stems from the first and second neighbours of the BCC lattice. Although the distances are different, it happens, due to different phase shifts, to stand at exactly the same position as the peak of nearest neighbours in pure Cu (see figure 4(*b*) or 5(*b*)). The second large peak, labelled II_{Fe}, originates from the fourth and fifth neighbours of the BCC lattice. Between these two peaks, the smaller peak corresponding to the third neighbours of the BCC lattice is correctly resolved only if the energy window is wide enough (40–430 and not 40–340 eV).

Figure 4 shows that in all irradiated samples, peak I is slightly shifted towards the low distances (by ~ 0.05 Å) while its amplitude is decreased as compared to that of the starting material; peak II_{Fe} decreases more rapidly and has entirely disappeared after a dose of 4.7 C cm^{-2} at 290 °C.

In the thermally aged samples (figure 5) the same evolution is observed up to ageing times of $\sim$ 8 h. For longer ageing times, a reverse evolution is observed so that peak I finally comes close to that of pure Cu. Peak II_{Fe} evolves differently from peak I. It does not grow again but instead completely disappears and for the longest ageing times (**FeCu** AG 312 h and to a lesser extent **FeCuMn** CR AG 115 h), the whole spectrum is close to that of pure Cu.

It is to be noted that, as long as only first and second neighbours are concerned, the 9R structure is identical to the FCC structure since any sequence of three nearest close-packed planes is the same in the two structures: as a consequence, peak I cannot evidence any difference between the 9R and the FCC phases. In contrast, some difference can be expected at higher distances since one sixth of the third neighbours and one third of the fourth and fifth neighbours must be different in the two structures; the shape of the spectra above 3.5 Å may be used to locate the transformation to the FCC phase. this transformation is almost achieved in **FeCu** aged for 312 h at 500 °C.

Table 2 gives the heights of peak I and peak II_{Fe} for the various samples (all determined with the smaller energy window: 40–340 eV).

Like the XANES data, the EXAFS data show that the Cu environment changes, as thermal ageing goes on, more rapidly in cold-rolled samples than in pre-annealed and quenched ones and that the change is more rapid in **FeCuNi** and **FeCuMn** than in **FeCu**. Due to the lack of data, such a comparison is difficult to make for irradiated samples. Not much difference is observed between **FeCu** and **FeCuMn** irradiated to a fluence of 4.7 C cm^{-2} at 290 °C.

4.2. Cr, Mn, and Ni thresholds

No change was observed at the Cr threshold in irradiated **FeCuCr** nor in thermally aged or irradiated **FeCuNi** at the Ni threshold. The Fourier transforms of the EXAFS spectra measured at the Mn threshold for **FeCuMn** samples are given in figure 6. The accuracy is much better than at the Ni threshold and a very slight change of peak II_{Fe} is observed at the Mn K edge for the longest ageing times (see table 2). No change beyond the experimental uncertainties was detected in any irradiated **FeCuMn** samples, including an Fe–0.3% Cu–1.5% Mn, irradiated with 0.5 C cm^{-2} at 290 °C.

5. Data analysis

5.1. Quantitative analysis of peak I

When it was possible, i.e. when the quality of the EXAFS spectrum at the Cu edge was good enough, we analysed peak I using the standard procedure: filtering, Fourier back

Table 2. Maximum height of the major peaks in the Fourier transform of the EXAFS spectra measured at the Cu (or Mn*) K edge.

	Peak I			*Peak II*$_{Fe}$		
Pure metals	Fe : .25 Cu : .20			Fe : .16		
Alloys	FeCu	FeCuNi	FeCuMn	FeCu	FeCuNi	FeCuMn
•Starting material						
CR	.23		.22 (.20*)	.15		.15 (.15*)
A Q		.20	.16 (.20*)		.15	.14 (.14*)
•Thermally aged						
A Q AG 2.5h	.22-.18-.17	.16-.16	.16-.17	.11-.13-.10	.08-.08	.07-.07
A Q AG 4.5h	.18	.15	.14	.08	.09	.07
CR AG 8h	.16			.07		
A Q AG 24h		.17			.05	
A Q AG 115h	.15			n. o.		
CR AG 24 h	.17		.19 (.19*)	n. o.		n. o. (.13*)
A Q AG 115h			.19 (.20*)			n. o. (.13*)
CR AG 115h		.18	.19 (.20*)		n. o.	n. o. (.12*)
A Q AG 246h		.22			n. o.	
A Q AG 312h	.20			n. o.		
•Irradiated						
CR $T_{irr} \approx 150°C$ 0.5 C/cm^2			.17			.09
A Q $T_{irr} \approx 240°C$ 0.5 - 0.6 C/cm^2	.20	.16	.18	.09	.08	.06
CR $T_{irr} \approx 230°C$ 0.5 C/cm^2		.17			.09	
A Q $T_{irr} \approx 300°C$ 0.6 C/cm^2	.15			.06		
CR $T_{irr} \approx 300°C$ 0.6 - 0.65 C/cm^2	.16		.15 - .16 (.20*)	.06		.04 - .06 (.14*)
A Q $T_{irr} \approx 290°C$ 4.7 C/cm^2	.16		.15 (.20*-.20*)	n. o.		n. o. (.135*-.135*)

n.o. stands for no longer observed. Several figures given together correspond to measurements on different samples of the same kind (i.e. same alloy, same ageing).

transformation and fitting. Peak I has been fitted assuming for the central atom one or two kinds of neighbour. We restricted to two the number of possibly different neighbours in order to maintain a reasonable number of fitting parameters. These near neighbours were assumed to be either (i) Fe atoms on a BCC lattice for Cu atoms in sold solution in Fe, or

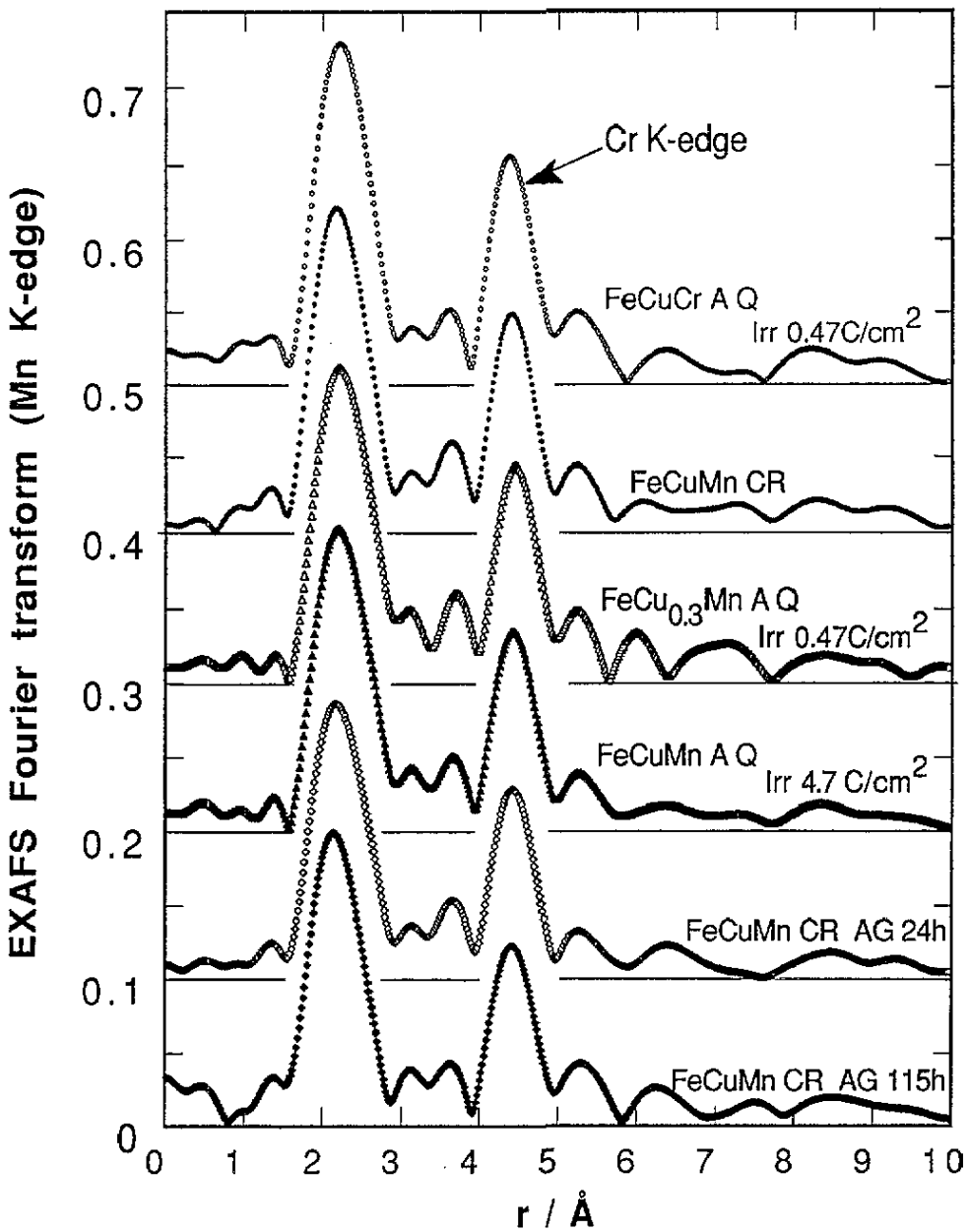

Figure 6. Fourier transform of the EXAFS spectrum at the Mn K edge for FeCuMn samples or the Cr K edge for one FeCuCr sample. CR stands for cold rolled, AQ for pre-annealed and quenched, Irr for irradiated at ~ 300 °C, and AG for thermally aged at 500 °C.

(ii) Cu atoms on a BCC lattice for Cu atoms in BCC clusters of Cu, or (iii) Cu atoms on an FCC lattice for Cu atoms in FCC clusters of Cu.

We thus had three sets of phase shifts (corresponding to these three possible environments of the Cu atoms) to determine. We deduced the back-scattered amplitudes and phase shifts of Fe and Cu first neighbours from Fe and Cu pure-metal spectra measured in the same conditions and analysed in the same way as the alloys.

As we have seen in section 4.1, peak I stems, for BCC structure, from the eight first neighbours and from the six second neighbours; since it is not possible to separate the contributions of these two shells, we determined an effective back-scattered amplitude for Fe atoms and an effective phase shift for Fe–Fe pairs by assuming one kind of 'average' neighbour, i.e. 14 first neighbours at a mean distance from the central atom of 2.65 Å instead of 2.48 and 2.87 Å. The effective phase shift of the Cu–Fe pair was obtained from that of the Fe–Fe pair by adding the difference between the two calculated central atom phase shifts (Teo and Lee 1979). The validity of the procedure is confirmed by the fact that a good fit is obtained for the CR and AQ starting material with 14 Fe first neighbours, as expected for Cu atoms in solid solution in the BCC Fe matrix.

To be able to calculate the first steps of the precipitation, we constructed an EXAFS spectrum for BCC Cu (with eight first neighbours at $r = 2.48$ Å and six second neighbours at $r = 2.87$ Å); this spectrum was calculated using the back-scattered amplitude and phase shift determined from the measured spectrum of FCC Cu metal (and assumed not to depend on the distance r in the range 2.48–2.87 Å). We then analysed this calculated spectrum in the same way as the experimental Fe metal spectrum (assuming 14 'average' Cu neighbours at $r = 2.65$ Å) and deduced an effective back-scattered amplitude and an effective phase shift for BCC Cu.

The effective back-scattering phase shift calculated for BCC Cu is very close to that deduced for BCC Fe. If we compare it to that determined for FCC Cu, we observe (figure 7) that it decreases more rapidly with k, compensating for the higher neighbour distance in BCC Cu (2.66 instead of 2.55 Å), so that peak I is found at about the same position for the three kinds of environment: BCC Fe, BCC Cu, or FCC Cu. If we now compare the effective amplitude back scattered by BCC Cu to that back scattered by BCC Fe (figure 7), we find it is 20–40% less between 100 and 300 eV (5–9 $Å^{-1}$). This explains the shrinkage of peak I in the first steps of precipitation (Cu precipitates coherent with the BCC matrix).

With the back-scattered amplitude and phase shift determined as mentioned above, we thus calculated the EXAFS signal given by one or two kinds of near neighbour, these neighbours being either BCC Fe, BCC Cu, or FCC Cu. The parameters of the calculation are the number n_i of atoms of the i^{th} kind contributing to the near-neighbour peak, their distance, r_i, to the Cu central atom, and the root-mean-square deviation σ_i from this distance; we assumed these deviations to be zero in the pure metals. The parameters were adjusted to best fit the filtered experimental spectrum, in the energy range 40–340 eV for **Fe**Cu and **Fe**CuNi samples and 40–430 eV for **Fe**CuMn samples. The obtained values are given in table 3. The label 'BCC' means that 14 'average' neighbours stand for the eight first neighbours and the six second neighbours of the BCC structure at a mean distance given in the next column. The total number of neighbours, $n = n_1 + n_2$, was first maintained constant (equal to 14 for BCC neighbours, 12 for FCC neighbours), and then allowed to vary within 10% of the expected value (to take into account the fact that the magnitude of the EXAFS signal is not determined with an accuracy much better than 10%). In most cases, the variation of n was small and did not result in any significant change of the best fit parameters.

For each sample, several different possibilities were tried. The values of the fit

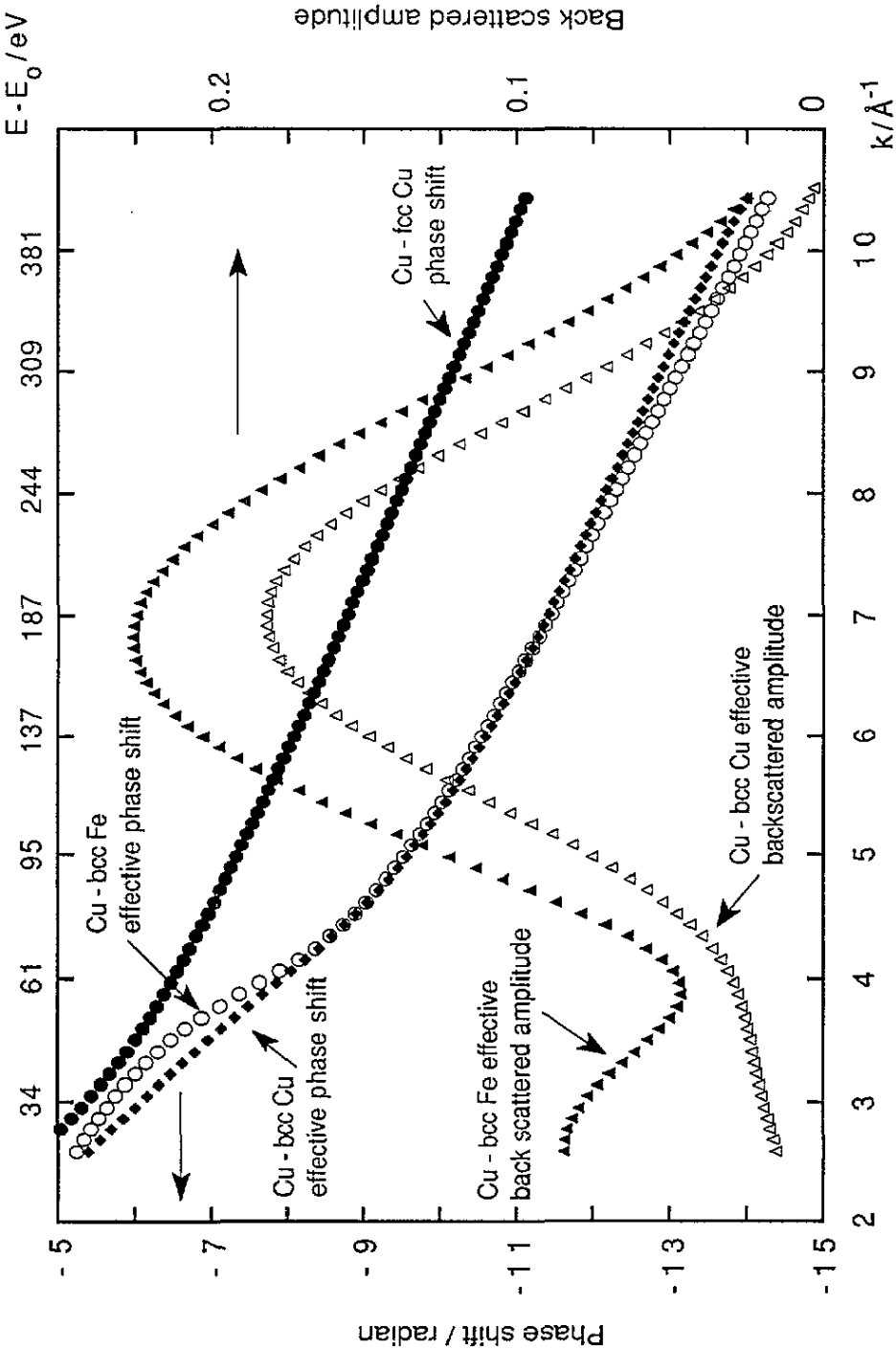

Figure 7. Phase shift and back-scattered amplitude for various near neighbours (BCC Fe, BCC Cu, and FCC Cu) of a Cu central atom, as a function of the electron wave number k or kinetic energy $E - E_0$.

Table 3. Analysis of peak I of the Fourier transform.

	First shell			Second shell			fit quality (%)	fcc (or 9R) fraction
	n_1	r_1/Å	σ_1/Å	n_2	r_2/Å	σ_2/Å		
FeCu								
CR	12.9 Fe bcc	2.65	.01	-	-	-	0.25	0%
A Q 0.6 C/cm² 300°C	*14 0 Fe bcc*	*2.66*	*.07*	-	-	-	*3.38*[F]	
	11.1 Fe bcc	*2.66*	*.05*	-	-	-	*(2.56)*	
	8.1 Fe bcc	*2.65*	*.01*	*5.9 Cu bcc*	*2.66*	*.15*	*2.74*	
	9.9 Fe bcc	*2.66*	*.05*	*1.8 Cu*	*2.55*	*.04*	*(2.57)*	
	8.0 Cu	2.50	.01	6.3 Cu	2.88	.15	0.78	0 %
A Q AG 2.5h	*14.0 Fe bcc*	*2.67*	*.04*	-	-	-	*1.75*[F]	
	11.9 Fe bcc	*2.67*	*.01*	-	-	-	*(0.85)*	
	5.0 Fe bcc	2.65	.00	9.0 Cu bcc	2.65	.01	0.71	0 %
	9.2 Cu	*2.50*	*.00*	*5.0 Cu*	*2.90*	*.00*	1.62	
CR AG 8h	8.5 Cu	2.49	.01	5.5 Cu	2.90	.14	0.18	10 %
A Q AG 115h	8.9 Cu	2.52	.01	3.0 Cu	2.88	.13	0.01	45 %
CR AG 24h	10.3 Cu	2.52	.02	3.2 Cu	2.89	.135	0.04	50 %
A Q AG 312h	11.4 Cu	2.55	.00	0.4 Cu	2.89	.06	0.15	95 %
FeCuNi								
A Q	14.0 Fe bcc	2.65	.05	-	-	-	1.08	0 %
A Q 0.55C/cm² 230°C	8.0 Cu	2.48	.00	6.0 Cu	2.89	.11	2.17	0 %
A Q AG 2.5h n°1	8.1 Cu	2.51	.00	6.3 Cu	2.89	.135	0.97	0 %
A Q AG 2.5h n°2	8.0 Cu	2.54	.00	6.0 Cu	2.89	.16	0.88	0 %
A Q AG 4.5h	7.6 Cu	2.49	.01	6.3 Cu	2.90	.15	1.54	0 %
A Q AG 24h	9.0 Cu	2.52	.01	4.0 Cu	2.89	.15	3.80	30 %
CR AG 116h	11.0 Cu	2.55	.01	1.5 Cu	2.95	.09	0.14	75 %
A Q AG 246h	11.5 Cu	2.53	.01	0.5 Fe bcc	2.68	.00	0.49	90 %
FeCuMn								
CR	14.0 Fe bcc	2.67	.03	-	-	-	1.00	0 %
A Q	14.1 Fe bcc	2.66	.06	-	-	-	0.76	0 %
CR 0.5 C/cm² = 150°C	8.0 Cu	2.48	.00	6.0 Cu	2.91	.08	1.52	0 %
CR 0.65 C/cm² 300°C n°1	8.2 Cu	2.50	.01	5.8 Cu	2.89	.16	1.18	5 %
CR 0.65 C/cm² 300°C n°2	8.0 Cu	2.49	.01	6.0 Cu	2.88	.15	0.38	0 %
A Q AG 2.5h n°1	8.6 Cu	2.51	.01	5.6 Cu	2.87	.16	0.10	10 %
A Q AG 2.5h n°2	8.7 Cu	2.50	.02	5.3 Cu	2.85	.21	0.78	10 %
A Q AG 4.5h	8.3 Cu	2.51	.03	5.7 Cu	2.88	.32	0.30	5 %
CR AG 24h	11.8 Cu	2.53	.02	1.2 Cu	2.90	.04	0.07	85 %
A Q AG 115h	10.4 Cu	2.55	.00	2.6 Cu	2.87	.01	0.53	60 %
A Q AG 115h Irr*	10.5 Cu	2.54	.00	2.4 Cu	2.87	.01	0.71	65 %
CR AG 115h	10.9 Cu	2.55	.00	1.8 Cu	2.87	.09	1.32	70 %

* this sample has received an electron dose of 0.55 C cm^{-2} at $\simeq$ 240 °C after thermal ageing.

[F] This means that the total number of neighbours was fixed; otherwise it did not maintain an acceptable value. The fit quality index is given in brackets when the total number of atoms is not acceptable, given an experimental uncertainty of $\simeq$ 10%.

The parameter values given in italics correspond to fits which are not the best ones, but are given as examples of what is obtained with different hypotheses.

parameters obtained in each case are given in table 3 for **FeCu** AQ irradiated with 0.6 C cm^{-2} at 300 °C and aged 2.5 h at 500 °C. (For all other samples, only the best fit is given in table 3). The fit quality depends on the spectrum quality (it is worse for **FeCuNi** than for **FeCu** spectra); it also depends on the homogeneity of the precipitate population and is never found to be very good for small ageings when the Cu atom environment is multiple and

when the surface of the precipitates is not negligible as compared to their volume.

In FeCu irradiated up to 0.6 C cm^{-2}, as in all samples irradiated up to a fluence of 0.6 C cm^{-2}, the best fit is obtained with 100% of the Cu atoms in BCC Cu precipitates; the lattice parameter of these precipitates is 2.89 ± 0.02 Å.

In most of the aged samples, the best fit yields two shells of Cu atoms around the central atom (and a negligible number of Cu atoms still in solid solution); the nearest-neighbour distance lies between the nearest-neighbour distance in the coherent BCC precipitates (2.49 ± 0.01 Å) and that in FCC Cu (2.55 Å). The second-shell radius is the second-neighbour distance of the BCC precipitates. We can thus conclude that, in these samples, BCC and FCC precipitates coexist and deduce from the values of n_1 and n_2 the fraction, $f = (3n_1 - 4n_2)/(3n_1 + 2n_2)$, of Cu atoms in an FCC (and/or 9R) Cu environment, since eight BCC first neighbours are to be there for every six BCC second neighbours. This fraction (last column of table 3), which is not determined with an accuracy better than ±10%, is comparable to that deduced from the XANES results (see table 1).

5.2. EXAFS structure above peak I

Between the first stage of Cu precipitation where peak II_{Fe} is still visible and its last stage where the spectrum clearly resembles that of Cu (as in **FeCu** AQ AG 312 h), the spectrum structure is intricate and cannot be considered as a simple combination of Fe and Cu spectra since such a combination yields a maximum between 4.2 and 4.4 Å. No maximum but rather a plateau is observed in **FeCu** AQ AG 115 h and **FeCu** CR AG 24 h (see figure 5). Now the radius of the precipitates, deduced from SANS experiments, is large enough (> 50 Å for **FeCu** AQ AG 115 h) *that the fraction of Cu atoms on the precipitate surface (< 20%) cannot* account for the lack of any defined structure around 4.3 Å. This lack can be interpreted as indicating the existence of another phase, intermediate between the BCC and FCC ones, possibly the 9R phase evidenced by transmission electron microscopy (Othen *et al* 1991). Table 4 gives the number of neighbours situated at a distance d from a given atom for the three structures BCC, 9R, and FCC. If one compares the 9R to the FCC structure, one sees a shift of the third and fourth neighbours towards small distances and a shift of the fifth neighbours towards large distances. This can explain the above-mentioned absence of a maximum around 4.3 Å, not taking into account the possible modifications of the phase shifts.

6. Discussion

In this section, we will summarize the results of the present XAS experiments and compare them with other results, mainly SANS results obtained with samples prepared and aged under the same conditions (Maury *et al* 1991a, Mathon *et al* 1993a). The only difference between XAS and SANS samples is their thickness (200–800 μm for SANS samples instead of 20–30 μm for XAS samples).

6.1. Precipitated atomic fraction and precipitate structure

The XANES and EXAFS data clearly show that, in **FeCu**, **FeCuNi**, and **FeCuMn** dilute alloys either thermally aged at 500 °C or electron irradiated around 290 °C, the Cu atoms are surrounded at the beginning of the precipitation by Cu atoms on a BCC lattice.

In one case only the present results indicated that the Cu precipitation was not complete: that of AQ **FeCu** aged for 2.5 h at 500 °C where only $70 \pm 10\%$ of the Cu atoms are found to

Table 4. Successive neighbours of a given atom in a BCC, 9R and FCC crystal. d is the distance between the pair and a_0 is the distance between nearest neighbours. The braces mean that the corresponding neighbours do not give rise to separate peaks in the Fe and Cu spectra, the brackets that they do not give rise to a distinguishable peak (given our energy window). The frame selects the atoms which are observed between 3.5 and 5.5Å in the copper spectrum.

d/a₀	bcc	9R	fcc
1	8	12	12
1.15	6		
1.41		6	6
1.63	12	4/3	
1.73		20	24
1.91	24	8	
2	8	8	12
2.24		16	24
2.31	(6)		
2.38		8	
2.45		6	(8)
2.52	24	6	
2.58	24	8	

enter Cu BCC precipitates, the remaining 30% being still in solid solution in the Fe matrix. This precipitated fraction is to be compared with that deduced from SANS data, $\sim$ 75%, and with the fractional resistivity loss for the same ageing time, 65%. The agreement is reasonable, taking into account the uncertainties in the EXAFS and SANS determinations. The mean radius of the precipitates, deduced from SANS, is $\sim$ 0.9 nm.

In FeCu electron irradiated with a fluence of 0.6 C cm^{-2} at 300 °C, all the Cu atoms ($\pm$10%) are found in BCC Cu precipitates. Their mean radius, determined by SANS, is then 2.3 nm. The lattice parameter of these BCC precipitates, deduced from a quantitative analysis of the first-neighbour peak, is 2.89$\pm$0.02 Å, a value very near to that of the matrix (2.87 Å) and slightly less than the value (2.96 Å) deduced from molecular-dynamics simulation by Phythian *et al* (1990).

After a thermal ageing of $\sim$ 150 h at 500 °C, which corresponds to a precipitate mean radius of 6$\pm$1 nm, about 50% of the precipitates are of BCC structure. Although the structure of the remaining 50% appears to be FCC as concerns the first neighbours, the shape of the EXAFS spectrum above the first-neighbour peak does not show the features expected for a simple combination of BCC and FCC structures. The complicated shape of the spectrum may reflect the existence of the 9R phase observed by Othen *et al* (1991).

After 312 h of thermal ageing at 500 °C, no more than 10% of the Cu precipitates are still of BCC structure (less than 10% if one takes into account the atoms at the interface with the matrix and, eventually, the residual solubility of Cu in Fe at 500 °C). A large fraction ($\geqslant \frac{3}{4}$) of the Cu precipitates have transformed to an FCC structure, as shown by the EXAFS spectrum structure above peak I. The mean radius of the precipitates is 7.95 $\pm$ 0.1 nm (Mathon *et al* 1993a), a value quite comparable to that deduced from high-resolution microscopy, which sees the intermediate 9R phase remaining stable up to 15 nm diameter (Phythian *et al* 1992).

6.2. Ageing of cold-rolled samples

We have seen (sections 3.1 and 4.1) that the fraction of FCC precipitates is found to be larger in a cold-rolled sample than in a pre-annealed and quenched one. The SANS data show that in irradiated FeCu (0.5 C cm^{-2} at 300 °C) the volumic fraction of precipitated Cu is smaller (by $\sim$ 30%) in the cold-rolled sample than in the annealed/quenched one. The resistivity

decrease is also much smaller in CR samples (see figure 1). Besides, the mean radius of the precipitates is found to be about equal in the CR sample and in the AQ one. The Cu precipitation thus appears to be rather hindered than promoted in the cold-rolled sample. However, a possible clue for explaining the larger fraction of FCC precipitates in this sample is the SANS indication that the precipitates may contain a few percent of vacancies or voids (which are not seen in the AQ sample): the Cu precipitates may have built preferentially on the dislocations, which could loosen the interaction with the matrix and facilitate the BCC → FCC transformation. Similar observations are made in **FeCuMn** AG 24 h: smaller volumic fraction and mean radius of the precipitates in the CR than in the AQ sample.

6.3. Effective of Mn

If we now compare **FeCu** and **FeCuMn**, the mean radius is found to be larger in **FeCuMn** than in **FeCu** (Maury *et al* 1991a, Mathon *et al* 1993a). The larger fraction of FCC precipitates in thermally aged **FeCuMn** as compared to **FeCu** observed in the present XAS experiments can thus be related to the larger size of the precipitates in **FeCuMn**.

The SANS data also show that in thermally aged **FeCuMn** samples and **FeCuMn** irradiated to a fluence of 0.5 C cm^{-2} at 300 °C, the precipitates contain $6 \pm 1.5\%$ Mn (or less if one assumes that they may also contain vacancies). The Mn content is found to be slightly larger ($10 \pm 2\%$) in **FeCuMn** irradiated to a fluence of 5 C cm^{-2} at 290 °C. These results are consistent with the present data, which show that at the Mn K edge, ageing or irradiation brings in only very slight modifications in the Fourier transform of the EXAFS spectrum (see figure 7 and table 2).

6.4. Comparison of radiation-induced and thermally induced precipitation

It has been observed from SANS data that **FeCu** irradiated samples behave, as concerns the mean radius of the precipitates, like thermally aged ones, 1 C cm^{-2} at 300 °C being equivalent to $\sim$ 10 h at 500 °C (Mathon *et al* 1993b). This relation holds also for microhardness and it seems applicable to the present data (see table 2b). Yet it is to be noted that such a simple equation may not hold for **FeCuMn**: the effect of Mn on the mean radius of the precipitates appears to be greater in the first stage of ageing.

A model has been developed for **FeCu** alloys by Smetniansky and Barbu (1993) based on the assumption that the main effect of the irradiation is to enhance the thermal precipitation by creating a vacancy concentration high enough to ensure the Cu migration.

Acknowledgments

We wish to thank F Faudot, S Peynot and P Ochin for preparation of the **FeCuNi** and **FeCuCr** alloys, C Bisson and P Laplace for technical assistance during thermal ageing and irradiation experiments, and the group in charge of the DCI machine for the x-rays. We also thank A Barbu for stimulating discussions.

References

Barbu A, Lé T N, Lorenzelli N, Maury F and de Novion C H 1992 *Mater. Sci. Forum* **97–9** 351

Beaven P A, Frisius F, Kampmann R and Wagner R 1986 *Atomic Transport and Defects in Metals by Neutron Scattering* (Berlin: Springer) p 228

Prisius F and Bünemann D 1979 *Proc. Int. Conf. on Radiation Behaviour of Metallic Materials for Fast Reactor Core Components (Ajaccio, 1979)* (Saclay: French Atomic Energy Commission) p 247

Hornbogen E and Glenn R C 1960 *Trans. Metall. Soc. AIME* **218** 1064

Lé T N 1992 *Thesis* Ecole Polytechnique

Little E A 1983 *Dimensional Stability and Mechanical Behaviour of Irradiated Metals and Alloys* (Brighton: British Nuclear Energy Society) p 141

Mathon M H, Maury F and de Novion C H 1993a

Mathon M H, Maury F, Dunstetter F, Lorenzelli N, de Novion C H and Boué F 1993b *9th Int. Conf. on Small Angle Scattering (Saclay, 1993); J. Physique* at press

Maury F, Lorenzelli N and de Novion C H 1991a *J. Nucl. Mater.* **183** 217

Maury F, Lorenzelli N, de Novion C H and Lagarde P 1991b *Scr. Metall.* **25** 1839

Müller J E, Jepsen O, Andersen O K and Wilkins J W 1978 *Phys. Rev. Lett.* **40** 720

Müller J E, Jepsen O and Wilkins J W 1982 *Solid State Commun.* **42** 365

Othen P J, Jenkins M L, Smith G D W and Phythian W J 1991 *Phil. Mag.* **64** 383

Phythian W J, de Diego N, Mace J and McElroy R J 1992 *Effects of Radiation on Materials: 16th Int. Symp. (Denver, CO, 1992)* ASTM STP 1175 ed A S Kumar, D S Gelles and K Nanstad (Philadelphia, PA: American Society for Testing and Materials)

Phythian W J, Foreman A E J, English C A, Buswell J T, Hetherington M, Roberts K and Pizzini S 1990 *UKAEA Harwell Report* AEA-TRS-2004

Pizzini S, Roberts K J, Phythian W J, English C A and Greaves G N 1990 *Phil. Mag. Lett.* **61** 223

Smetnianski N and Barbu A 1993 to be published

Soulat P and Meyzaud Y 1990 *Mem. Et. Sci. Rev. Métall.* **87** 769

Teo B K and Lee P A 1979 *J. Am. Schem. Soc.* **101** 2185

Worrall G M, Buswell J T, English C A, Hetherington M G and Smith G D W 1987 *J. Nucl. Mater.* **148** 107